Inductively Coupled Plasma Sputtering: Structure of IV-VI Semiconductors

S.P. Zimin
Yaroslavl State University, Yaroslavl, Russia

E.S. Gorlachev

I.I. Amirov
Yaroslavl Branch of the Institute of Physics and Technology of Russian Academy of Sciences, Yaroslavl, Russia

Abstract
In this entry, we describe the latest results on application of high-density inductively coupled argon (Ar) plasma sputtering for the nanostructuring of IV–VI semiconductors. We analyze the main physical processes that take place during inert gas plasma sputtering of lead chalcogenide layers, evaluate sputtering yields of these materials in the framework of the Sigmund's model, and present novel approaches to the fabrication of lead chalcogenide nanostructures, such as nanohillocks, nanocones, nanocubes, and high aspect ratio nanowires, using inductively coupled Ar plasma sputtering.

INTRODUCTION

The binary lead chalcogenides PbX (X = Te, Se, S) and PbX-based ternary solid solutions represent one of the most important groups of narrow-gap IV–VI semiconductor materials that are widely used in modern solid-state electronics in the production of infrared optoelectronic and thermoelectric devices. Historically, IV–VI semiconductors, and lead chalcogenides in particular, were one of the first actively studied semiconductor materials, for which research laid the foundations of the physics of semiconductors and semiconductor devices. By now, there is quite a good understanding of the properties of lead chalcogenides, and there are various effective methods of PbX single crystal growth and of the formation of single-layer and multilayer film structures (superlattice structure with quantum wells) with unique physical properties.[1,2] The interest in lead chalcogenides sharply increased due to new opportunities emerging in the transition of these materials into the nanometer range. Specific properties of lead chalcogenides associated with small effective masses of carriers and high permittivity make them a promising group of semiconductors for the realization of the size quantization conditions and localization of carriers.[2] The transition to the quantum size effects in these materials is carried out at dimensions of 30–50 nm (under certain conditions up to 150 nm), while for silicon (Si), it is necessary to achieve a size less than 4–5 nm. The first publications on the creation of low-dimensional PbX systems and quantum size effects studies have appeared already in the 1970s–1980s.[3–5] Expanding experimental research and active development of nanotechnology enabled to apply nanostructured lead chalcogenides in the growing fields of photovoltaics,[6,7] optoelectronics,[8,9] nanoelectronics,[10] thermoelectric devices,[11] and medical bioimaging.[12,13] Much attention is being paid to the improvement of the functional characteristics of semiconductor materials based on lead chalcogenides (thermoelectric figure of merit, transmission spectra, reflection spectra) by applying PbX elements with nanometer size to solid substrates or by their introduction into a gaseous, liquid, or solid medium. The development of new methods for the synthesis of nanostructured PbX is an urgent task of modern technology. One of the most prospective approaches to nanostructuring is a "top-down" technique via dry etching using ion beam or ion plasma treatment. The first studies on ion etching of IV–VI materials were not directly intended for nanostructuring and were conducted for various aims: for formation of heterostructure laser waveguides,[14] for fabrication of submicron mesa structures using ion milling[15,16] or gas mixture plasma etching,[17] and for surface cleaning.[18] It is important to notice that a detailed complex study of dry etching process for IV–VI materials was never carried out. In this entry, we discuss physical processes that take place during treatment of lead chalcogenide layers in high-density inductively coupled plasma (ICP) reactor and examine new possibilities of fabrication of PbX nanostructures using ICP sputtering, which is an extremely important matter during the transition to nanotechnology tasks within the

Encyclopedia of Plasma Technology DOI: 10.1081/E-EPLT-120053966

expansion and modernization of the traditional Si technology.

THE BASICS OF ICP REACTOR SETUP AND SAMPLE TREATMENT

Radio-Frequency (RF) ICP Discharge Sources

Sputtering of various materials with inert gas ions using a mask process is simpler and can be easily implemented in plasma chemical reactors that are used in microelectronics technology. In such setups, all the processes take place at low pressures ($p < 10$ Pa), and unlike the previously used high-frequency capacitive plasma source reactors, modern plasma chemical reactors allow to independently control the energy and the ion flux of the ions bombarding the substrate surface. Even at low energy of the incident ions ($E_i < 500$ eV), the substrate sputtering rate can be quite large due to the high density of the ion flux. Since the removal of the substrate material is determined by physical ion bombardment, the anisotropic etching must be high. There are several types of sources of high-density low-pressure plasma developed.[19,20] Among these, the most common and versatile are the reactors with solenoidal and planar RF ICP discharge sources (Fig. 1). Using a second RF generator, from which the RF power is supplied to the RF electrode, enables to control the energy of the ions bombarding it. The difference in these types of reactors is in the transport of plasma from the generation zone toward the substrate. In a reactor with a flat RF inductive discharge (Fig. 1A), the substrate is located on the RF electrode near the plasma generation area. Plasma chemical reactors with such RF plasma sources are produced by different firms (e.g., Oxford Instruments, Lam Research, and Applied Materials).

Plasma reactor with an RF solenoidal inductive discharge consists of two chambers: the discharge one and the reaction one (Fig. 1B). RF ICP discharge generated in the discharge chamber usually via a magnetic field extends into the reaction chamber, where a treated sample is placed on the electrode. Application of a magnetic field increases the plasma density. The density of the ion flux is determined by the RF power applied to the inductor, and the energy of ions—by the RF bias power P_{sb} applied on the electrode (substrate holder). The generated plasma is characterized by high uniformity of ion flux on the substrate surface. The frequency of the applied RF field is typically 13.56 MHz. For the following typical parameters of the discharge: $p = 0.1$–10 Pa and $P_{sb} = 600$–2000 W, the ion current density on the surface is 1–20 mA cm^{-2}, and the ion energy varies from 20 eV to 1 keV.

Basics of Surface Sputtering (Dry Etching) in RF ICP Reactors

In RF ICP reactors, the surface of a sample placed in the plasma undergoes ion and electron bombardment. Since the mobilities of ions and electrons are radically different, but the fluxes of ions and electrons at the substrate are the same, and the insulated substrate is being negatively charged to the floating potential level. Near the substrate there takes place a formation of a space charge layer (sheath), wherein positive ions are accelerated to the energy

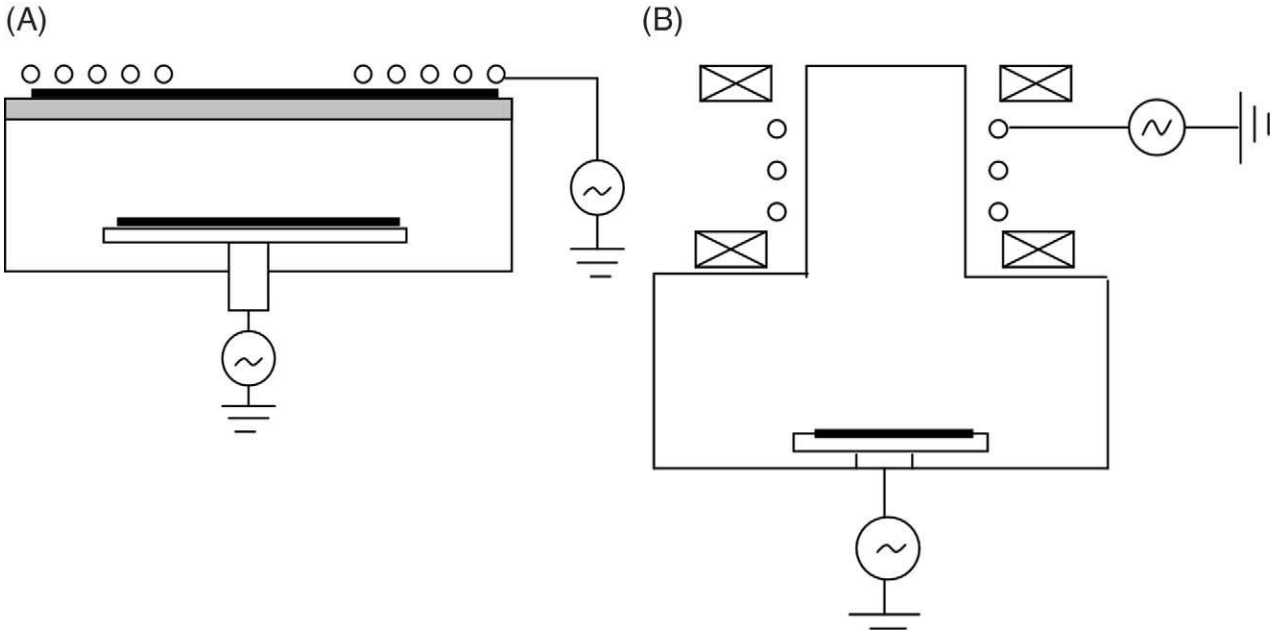

Fig. 1 Basic construction types of high-density RF ICP reactors: Flat discharge reactor (A) and solenoid discharge reactor (B).

determined by the difference between the plasma potential and the floating potential. The ions fall vertically to the surface with the energy determined by the electron temperature T_e. The electron temperature is usually 3–7 eV, and the ion energy is 20–40 eV.[19] In order to increase the energy of the bombarding ions, an independent RF power bias of 0–400 W from a stand-alone RF generator is applied on the aluminum (Al) electrode (substrate holder). Thus, on the electrode, a negative self-bias potential is formed, which determines the average energy of the incident ions. The average energy of the bombarding ions is linearly proportional to the RF power applied to the substrate holder in accordance with the increase in negative self-bias potential arising on the electrode.

Using inert gas [primarily, argon (Ar)] plasma for ICP dry etching allows virtually eliminating chemical etching processes and providing physical sputtering of the surface region of the films. Simple chemistry of Ar plasma (a gas of electrons, Ar atoms, and Ar^+ ions bombarding the substrate) and chemical inertness make Ar gas suitable for the study of processes of plasma sputtering of solids. The basis of the plasma processing in this case is the impact energy of the Ar^+ ions to the substrate, which leads to the material removal (dry etching) in the form of atoms, molecules, and clusters via physical sputtering without any chemical processes or selectivity. In this situation, the sputtering would occur when the Ar^+ ions have energies higher than the target surface binding energy (sublimation energy). The advantages of plasmas generated in RF ICP reactors are low operating pressure, high plasma density, high flux density of ions, independent control of ion energy by changing the RF bias, uniform direction, and low energy spread of the ions.

ICP reactor used for IV–VI semiconductors sputtering

Experimental studies of PbX film sputtering processes were carried out on the setup, which included a plasma chemical reactor with vacuum air lock, a sample loading apparatus, a pumping system, and also vacuum and gas control systems. The pumping system consisted of a turbomolecular pump (400 l s^{-1}), a fore-vacuum pump, an automatic diaphragm, and pneumatic valves. Minimal residual pressure in the reactor was 2×10^{-4} Pa. The operating pressure was measured using capacitance manometer MKS Baratron (MKS Instruments, Andover, Massachusetts, USA). Plasma was generated in a high-density RF ICP discharge reactor (Fig. 2). The reactor consisted of the discharge chamber (1) and the reaction chamber (2). Plasma was generated in the discharge chamber in the cylindrical (diameter and length = 100 mm) quartz cup using a double-turn inductor (3) and an RF generator (P = 1 kW, f = 13.56 MHz) with a

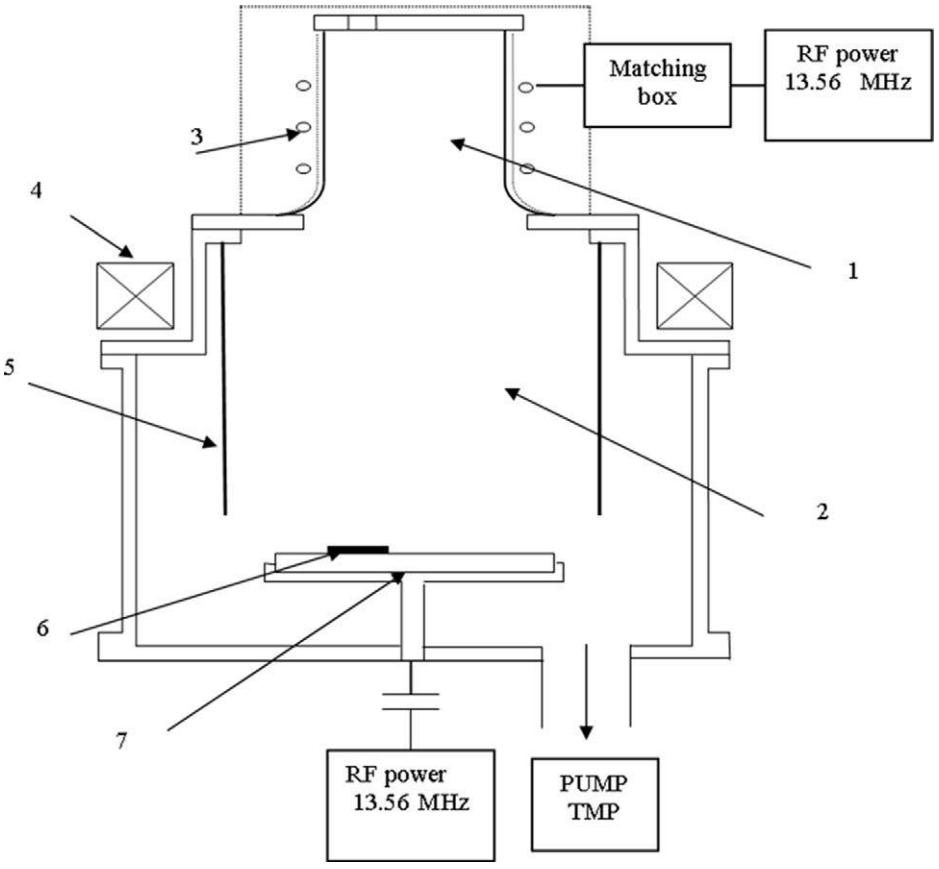

Fig. 2 Schematic of the RF ICP solenoid discharge reactor: 1—discharge chamber, 2—reaction chamber, 3—inductor, 4—electromagnetic coil, 5—thin-walled Al cylinder, 6—sample, 7—water-cooled RF electrode.

matching box. From the discharge chamber, the plasma was distributed in a metal reaction chamber, in which at a distance of 300 mm from the lower edge there was located a water-cooled Al RF electrode with a diameter of 150 mm (7). Using the loading apparatus, on the electrode, there was placed an Al plate (diameter = 150 mm, thickness = 2 mm) serving as a sample holder (6). Independent RF generator (P_{sb} = 0–600 W, f = 13.56 MHz) was applied to the electrode. The zone of plasma generation and propagation was in inhomogeneous magnetic field generated by electromagnetic coil (4). Inside the reaction chamber, there was installed a thin-walled (thickness = 0.75 mm) Al cylinder (diameter = 220 mm), which limited the plasma discharge volume.

The main parameters of the ion flux are its composition, density, and functions of the ion energy and angular distribution. It is well known that in ICP discharges it is possible to independently control the energy of the ions and the ion flux.[21,22] The ion flux is determined by the RF power P applied on the inductor, and the ion energy is controlled by the RF bias power P_{sb} applied on the substrate. The application of the RF bias power on the electrode results in the emergence of the negative self-bias potential U_{sb}, which controls the energy of the bombarding ions. The function of the ion energy distribution (IED) on the substrate surface for RF ICP has a double energy maxima and not a monoenergetic single-peak shape, as in the case of the constant negative potential on the electrode.[23–25] In general, the IED shape depends on the ion mass and the frequency of the applied RF field.[24] The IED width is calculated as the peak-to-peak electrode voltage $V(el)_{PP}$ minus the peak-to-peak plasma voltage $V(plasma)_{PP}$:[25]

$$\text{IED width} \approx V(el)_{PP} - V(plasma)_{PP} \tag{1}$$

Experimental measurements of the IED and self-bias potential in the RF ICP reactor showed that the U_{sb} is positioned symmetrically between the two maxima of the IED curve.[24] Therefore, it can be assumed that the average ion energy is determined by the self-bias potential. Knowing the average ion energy, it is possible to determine another main characteristic of the plasma sputtering—the ion current density J. It was calculated from the dependence of self-bias potential on the applied RF power. When the entire RF bias power applied to the discharge is expended on the acceleration of the ions in the sheath, it can be assumed that $P_{sb} \sim JU_{sb}$ for the electrode with area S.[22] Hence,

$$J = \frac{\Delta P_{sb}}{\Delta |U_{sb}| S} \tag{2}$$

It should be noted that, of course, not the entire RF power is spent for the acceleration of the ions, since a certain percentage of it can be lost in a coupling device. It is believed that in the case of a full coupling up to 95% of applied RF power can be transmitted to plasma.[26] Typical value of ion current density J calculated using Eq. 2 during our experiments was in the range of 5.5–7.5 mA cm^{-2}, which corresponded to the value of ion flux F_i of 3.4–4.7 × 10^{16} ion cm^{-2} s^{-1}.

In plasma, the function of the angular distribution of the incident ions had the appearance of a normal distribution:[27]

$$\psi(\xi) = \frac{1}{\sigma\sqrt{2\pi}} \exp\left(\frac{-\xi^2}{2\sigma^2}\right) \tag{3}$$

where σ is the root-mean-square angular deflection of ions. The value of σ was considered equal to the width of the angular distribution of ions σ_i, which depends on the energy of the plasma and ion temperature T_i:[28,29]

$$\sigma_i = \text{arctg}\left(\sqrt{\frac{kT_i}{E_i}}\right) \tag{4}$$

where k is Boltzmann constant, and E_i is the ion energy. The value of kT_i in plasma does not exceed 0.2 eV.[29] For kT_i = 0.2 eV and E_i = 90 eV, σ_i value is 2.7°. An example of the formation of IV–VI microstructures on the surface of lead selenide (PbSe) layer on Si substrate using Ar plasma sputtering with a metallic chromium mask is presented at Fig. 3. Formation of microcones on the surface, as well as the emergence of sloped rather than vertical sidewalls, is explained by the process of the sputtered material redeposition on the walls and by the not monotonic dependence of the sputtering yield on the incident angle.

SPUTTERING RATES AND SPUTTERING YIELDS OF IV–VI SEMICONDUCTORS IN ICP

Investigations of Sputtering Rates of Lead Chalcogenides in Inductively Coupled Ar Plasma

Sputtering rate is the main parameter of plasma etching of different materials. Its study is important from both fundamental and practical viewpoints, with the latter being a key in the micro- and mesa-multilayered devices fabrication. For the study of PbX sputtering rates, we used epitaxial films of binary compounds lead telluride (PbTe), PbSe, and lead sulfide (PbS) grown by molecular beam epitaxy on Si(111) or BaF_2(111) substrates.[30–32] In the former case for the lattice parameter mismatch compensation between the film and the Si substrate, the calcium fluoride (CaF_2) buffer layer with the thickness of 2–4 nm was used. The substrate temperature during film growth was 350–400°C. The thickness of the PbX films was 1–5 μm, and they had the orientation (111) along the growth axis and were characterized by a monocrystalline structure. The main experiments on the PbX film sputtering in Ar plasma were carried out in the

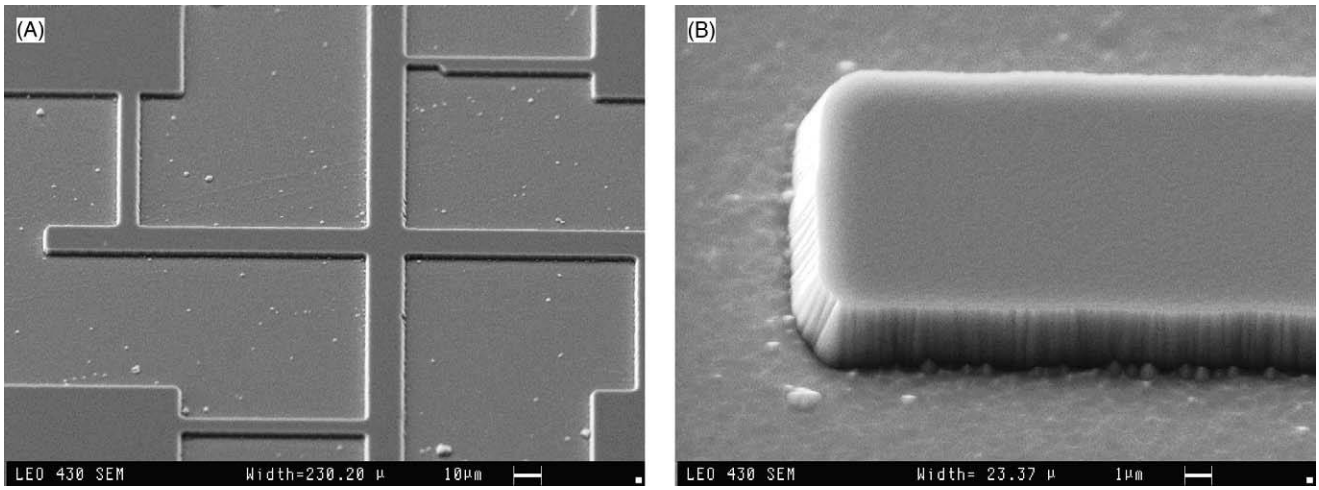

Fig. 3 PbSe microstructures fabricated using argon RF ICP sputtering with a chromium mask.

RF ICP reactor with the following parameters: P_{sb} = 200 W, E_i = 150 eV, Ar gas flow Q = 10 sccm, p = 0.08 Pa, J = 5.5 mA cm^{-2}, and $F_i = 3.4 \times 10^{16}$ ion cm^{-2} s^{-1}. The sputtering etch rate of the films was determined by the etch step measurement using Talystep profilometer (Taylor Hobson, UK). The etch step was obtained using a Si wafer stencil mask. The etch step height depended linearly on the treatment duration in the time range of 30–120 s, indicating that the sputtering rate of PbSe, PbTe, and PbS films was constant in time. Reported measurements of the temperature of a Si wafer showed that it is heated to ~500 K after 30-s plasma treatment with the P_{sb} = 200 W.[33] We have found out that the etching step heights for the thermostated PbX/CaF_2/Si(111) and PbX/BaF_2(111) samples placed on massive sample holder using vacuum glue and for the free-laying samples were identical, which indicates the independence of the sputtering rate on the temperature.

The results of our experimental measurements of the sputtering etch rate V for the PbX binary compounds during sputtering in Ar RF ICP with average Ar^+ ion energy E_i = 150 eV were as follows: for PbTe V = 10.4 ± 0.3 nm s^{-1}, for PbSe V = 8.9 ± 0.3 nm s^{-1}, and for PbS V = 8.8 ± 0.3 nm s^{-1}.[34] These values are close and are strongly surpassing the sputtering rates for other well-known binary semiconductors. Thus, the values of the sputtering rate for PbX reduced to the ion current density of 1 mA cm^{-2} are in the interval of 1.6–1.9 nm s^{-1}. The reduced sputtering rates for Si,[35] InN,[36] GaN,[37] InSb,[38] and GaAs[39] for the Ar^+ ion sputtering under similar conditions are noticeably smaller and are 0.02, 0.2, 0.4, 0.6, and 0.7 nm s^{-1}, respectively.[34]

Analysis of Sputtering Yields of Lead Chalcogenides in the Framework of the Sigmund's Model

The main parameter describing the effectivity of the process of the interaction of ions with a solid substrate is the sputtering yield Y, which shows how many atoms are leaving the surface due to the impact of a single bombarding ion. For an experimental determination, the sputtering yield Y of a material consisting of one kind of atom is calculated using:[40]

$$Y(\text{atom/ion}) = \frac{V\rho eN_A}{JM} \quad (5)$$

where ρ is the density of the studied target, N_A is the Avogadro constant, M is the molecular mass of the target. In case of polyatomic targets, the overall sputtering yield Y in general will be determined by the sputtering yields and the concentrations of the atoms of each kind.[41–44] In contrast to other compound semiconductors, for lead chalcogenides, the values of the molecule dissociation energy in the crystalline and gaseous states exceed the values of the sublimation energy E_{subl} at 298 K, and the degree of the molecule dissociation is only a few percent.[45–47] As a result, during the sputtering of lead chalcogenides, entire molecules are being physically sputtered from the surface instead of individual atoms.[34,46]

In case of the sputtering of the entire molecules, for the determination of the sputtering yield Y, it is possible to modify Eq. 5 by inserting the values of the density and the molecular mass for PbX compounds:

$$Y(\text{molecule/ion}) = \frac{V\rho_{PbX}eN_A}{JM_{PbX}} \quad (6)$$

The calculated PbX sputtering yields for the energy of Ar^+ ions of 150 eV (P_{sb} = 200 W) were as follows: for PbTe Y = 0.45 ± 0.02 molecule/ion, for PbSe Y = 0.44 ± 0.02 molecule/ion, and for PbS Y = 0.49 ± 0.02 molecule/ion (we describe this in more detail in Zimin et al.[34]). Thus, for all PbX compounds, Y is in the narrow range of 0.46 ± 0.05 molecule/ion, which is significantly smaller than the sputtering yields of individual atoms.[48] As a result, the concentrations of

lead (Pb) and chalcogen on the surface of the initial and the plasma-treated films remain approximately constant, as confirmed by energy-dispersive X-ray (EDX) microanalysis.[34]

Obtained results of the close values of the sputtering yields for the binary lead chalcogenide compounds qualitatively can be explained in the framework of Sigmund's model[49] of a sputtering of a random monoatomic target in the linear collision cascade regime, additionally making a substitution of the sputtered atoms of one kind by the molecules of one kind. For the sputtering yield with an ion energy of $\sim$1 keV, Sigmund has obtained a general equation:[49]

$$Y = \frac{0.042\alpha S_n(E_i)}{U_0} \quad (7)$$

where α is the factor depending on the ratio of the masses of the target atoms (molecules) and of the primary ion, $S_n(E_i)$ is the nuclear stopping cross-section, U_0 is the surface binding energy (sublimation energy). The replacement of the chalcogen X in PbX does not significantly change the value of αS_n due to a lower mass with respect to Pb, and the values of U_0 (or E_{subl}) of the lead chalcogenide binary compounds are close and differentiate at most by 6%.[34] Thus, the close Y values are explained by the similarity of the chemical and thermodynamic properties of lead chalcogenides and the small ratio of the mass of the primary Ar ion to the mass of the sputtered molecule.

As a conclusion, we should note that the main characteristic of the RF ICP etching of lead chalcogenides is the sputtering of individual molecules,[34] which allows minimizing segregation processes in the surface layer and applying classical models for the qualitative analysis of the sputtering features, such as close sputtering yields. The proposed models were further confirmed in the studies of plasma sputtering of ternary solid solutions $Pb_{1-x}Eu_xSe$, $Pb_{1-x}Sn_xTe$.[50,51]

NANOSTRUCTURING OF IV–VI SEMICONDUCTORS USING INDUCTIVELY COUPLED AR PLASMA SPUTTERING

Micromasking and Nanohillock Array Formation Effects during ICP Treatment of Lead Chalcogenide Layers

For nanostructuring experiments, we used epitaxial films of lead chalcogenide binary and ternary solutions PbTe and PbSe on CaF_2/Si(111) substrates. The utilization of Si substrates is advantageous as it offers compatibility with many other processing technologies. Epitaxial films with thickness of 1.5–5 μm were grown with molecular beam epitaxy on Si(111) substrates using a 2-nm thin CaF_2 buffer layer.[30,32] For the employed films, the density of threading dislocations was 1×10^7–4×10^8 cm^{-2}. Their initial surface was characterized by the presence of triangular pits of dislocation exits and triangular nanoterraces formed due to the dislocation glide in the <011>{001} glide system during a relaxation of thermal mismatch strain.[30,52] PbX film surface treatment was carried out in Ar RF ICP with p = 0.07 Pa, Q = 5 sccm, and P_{sb} = 200–400 W. Standard treatment time was 30 seconds.

It was established[30–32,53] that during the plasma treatment a selective sputtering of the surface of the PbX layers takes place, which results in a significant microrelief modification. Plasma-treated film surface was characterized by two groups of structures: submicrometer-size hillocks (microhillocks) and nanometer-size hillocks (nanohillocks) (Fig. 4). Strict compliance of the microhillock density with the dislocation density in the layers, as well as the presence of dislocations exit pits on hillock tops, suggests that the microhillocks are localized at the exits of threading dislocation of the epitaxial layer.[30,31] Microhillocks' maximum height corresponded to the thickness of the sputtered layer, which was 150–450 nm, and was linearly dependent on the duration of plasma processing. Nanohillocks had a height of 10–50 nm and typical surface density of 1–4 $\times$ 10^9 cm^{-2}, which corresponded to the density of the apexes of the triangular terraces on the initial surface.[30]

The effect of microhillock formation can be suppressed by increasing RF bias power;[31] however, in such case, it is accompanied by an undesirable growth of ion energy and sputtering rate. Generally, microhillock formation is a negative effect, since they are harmful to upper layers. It is well known that during plasma treatment the microhillock formation is usually related to the process of micromasking of certain surface areas with low-volatile compounds preventing them from sputtering.[54] Micromasking effect, which is well known for plasma treatment of Si[55,56] and other semiconductor materials,[57,58] consists in the presence of local self-assembled micromasks on the substrate surface with the sputtering rate much smaller than that of the substrate, which therefore prevent the underlying areas of the substrate from sputtering. Due to the angular sputtering rate dependence and redeposition, the conical or hillock-like structures are consequently formed with micromasks on their tops. To date, it is well established that the main source for micromasking material in ICP plasma sources is Al, which is sputtered from the surface of the sample holder and aluminum oxide chamber walls and is consequently redeposited on the sample surface. Comparative secondary ion mass spectrometry investigations of lead chalcogenide (PbSe) films after their plasma treatment when placed on Al or Si wafer holders showed that the Al and fluorine (F) concentrations were found to be increased for the sample situated on Al holder.[53] The presence of trace concentrations of F could be connected with the sputtering of previously contaminated chamber walls.[59] The simultaneous presence of F and Al results in

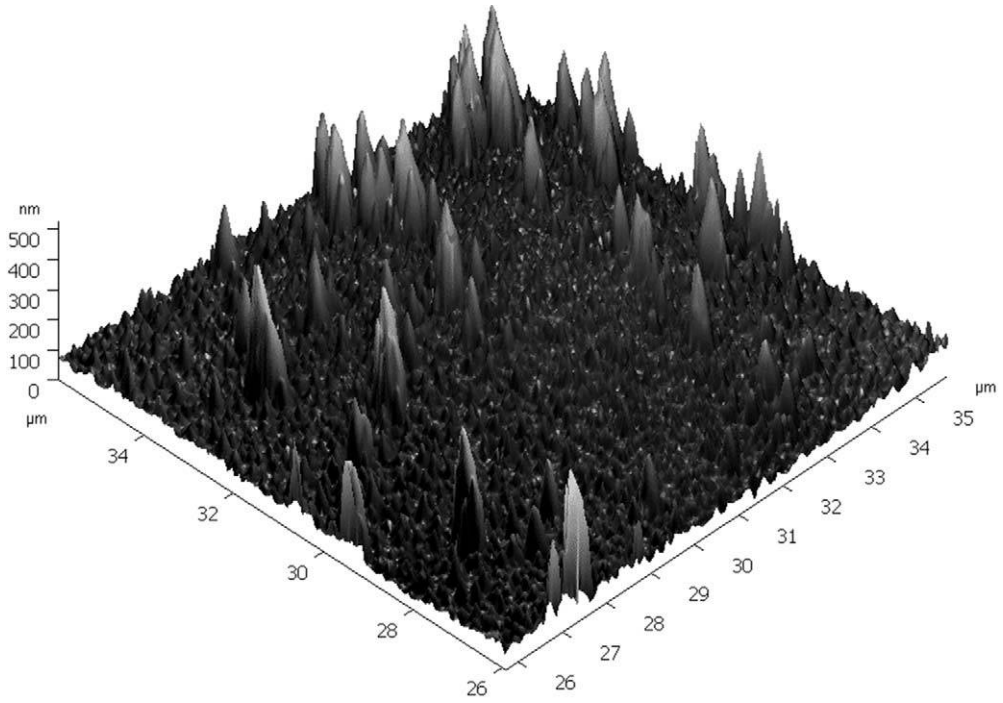

Fig. 4 Atomic force microscopy image of PbTe microhillocks and nanohillocks on the surface of PbTe film on CaF_2/Si(111) substrate modified using inductively coupled argon plasma treatment. Scan area is 10 × 10 μm^2.

strong micromasking, since Al–F compounds are stable and extremely low-volatile materials.[55] In case of Al electrode sputtering, ionized Al-containing particles could be preferably localized at the dislocation areas due to a built-in dislocation line charge. Then, during plasma treatment, such micromasking particles, self-positioned on the dislocation exit sites, result in the formation of microhillocks, which consist of the unsputtered underlying material.[54] Atomic force microscopy studies using spreading resistance imaging with a conductive tip in contact with the sample surface showed that the tops of the hillocks with triangular pits are conductive.[53] The resistivity value in the growth direction of $Al_{1-x}F_x$ nanolayers, formed via plasma sputtering, is at the level of 10^{-3} Ohm cm.[60] Considering the fact that PbTe or PbSe resistivity exceeds this value by several orders of magnitude, the appearance of high-conductive phase on the microhillock tops is becoming explainable and thus supports the model of Al–F serving as micromask of the dislocation areas.[53] On the other hand, F could potentially react with Pb, which is segregated in the Cottrell atmospheres of dislocations.[61,62] The physical model of dislocations micromasking during plasma processing of PbX films is presented in Fig. 5.

On the basis of the results reported above, we developed and realized a novel plasma treatment method for the fabrication of lead chalcogenide nanostructures on Si substrates. Considering the abovementioned experimental results, we had to exclude any F from the plasma chamber so that the micromasks would not be generated and also to reduce the sputtering rate in order to minimize the thickness of the sputtered layer. The RF ICP chamber prior to use was cleaned in oxygen plasma, and Si wafer was used as a sample holder. Plasma treatment parameters were as follows: Q_{Ar} = 100 sccm, p = 1.2 Pa, P_{sb} = 0 W, and duration = 1–5 minutes. As a result, a formation of arrays of uniform nanostructures took place without any micromasking effects (Fig. 6). Density of nanohillocks for

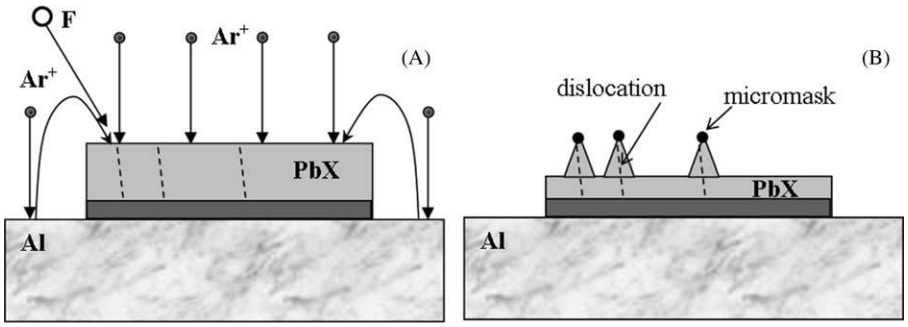

Fig. 5 Dislocation micromasking model for the PbX plasma sputtering: (A)—initial PbX film on Si substrate and Al substrate holder, (B)—modified PbX film after argon plasma treatment.

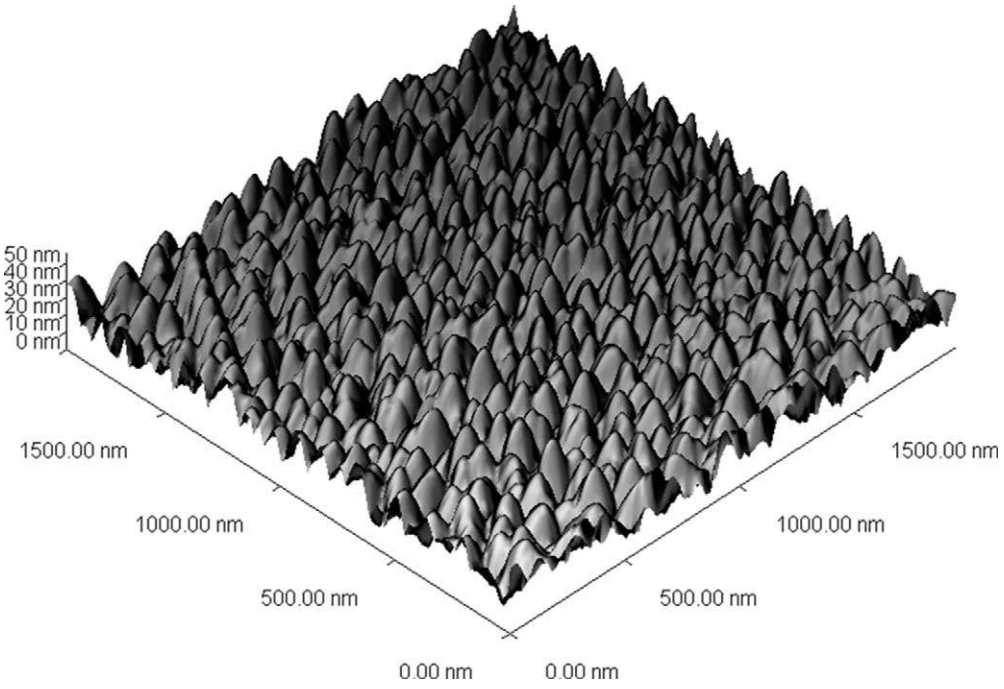

Fig. 6 Atomic force microscopy image of PbSe nanostructures obtained by inductively coupled argon plasma treatment of PbSe/CaF_2/Si(111). Scan area is 2×2 μm^2.

various PbX films was 1×10^9 cm^{-2}–4×10^9 cm^{-2}. Nanohillock average half-width was 80 nm, and mean height was 10–25 nm with a standard deviation of 45–50%.[53] This straightforward approach allowed us to create nanostructures on the PbX film surfaces, whose parameters are close to the conditions of dimensional quantization[63] and comparable with the structure sizes obtained with more expensive "bottom-up" molecular beam epitaxy methods.[64] A mechanism of the nanohillock arrays formation, according to the contemporary concepts of plasma-aided nanofabrication[65,66] is, most probably, a combination of "top-down" processes (physical sputtering) and "bottom-up" self-organization (PbX molecule redeposition and surface diffusion).

Fabrication of IV–VI Semiconductor Nanowire Arrays Using Redeposition Processes during Inductively Coupled Ar Plasma Sputtering

Fabrication of PbSe nanowires on PbSe/CaF_2/Si (111) substrates

From the examination of the results of the previous sections, it follows that the PbX layers, having high sputtering rates in ICP, should be able to create a high density of vapor of sputtered molecules at the surface, which potentially could be used for aimed nanostructure fabrication. We have suggested a new approach to PbX nanostructure fabrication inside a microgap under a stencil Si mask on a PbX layer, where the physical sputtering processes are absent, but there is a high vapor density of sputtered PbX molecules and high temperature, thus providing the necessary conditions for the catalytic growth via a vapor–liquid–solid mechanism.[67]

The initial samples were PbSe films with 1.7 μm thickness on CaF_2/Si(111) substrates that were treated in Ar RF ICP with P_{sb} = 200–400 W. A characteristic feature of these experiments was the use of a stencil mask, which was a monocrystalline Si wafer with a thickness of 380 μm with through periodic round holes with a diameter of 75 μm. It was applied in such a way that there was a microgap between the mask and the PbX film with a size of about 10 μm. During sputtering, in the open areas, the PbSe film was fully removed, but the Si substrate remained virtually unsputtered. A new phenomenon taking place during this process was a formation of 1-D nanostructures on the surface of the PbSe film under the stencil mask in the immediate vicinity of the sputtered areas.[67] Typical image of such nanostructures is shown in Fig. 7. The height of the cylindrically shaped nanowires reached 1000–1200 nm at a diameter of 75–125 nm. On the tops of nanowires, there were quasi-spherical faceted structures with 85–180 nm diameters. The surface density of nanowires was 1×10^9 cm^{-2}–2×10^9 cm^{-2}. On the areas of the surface of PbSe film under stencil mask and removed from the area of plasma treatment at a distance over 20–30 μm, instead of nanowires there took place a formation of spherical nanostructures. They have a diameter of 38–78 nm, and their density decreased with increasing distance from the sputtered area: 2×10^9 cm^{-2} for a distance of 750 μm and 4×10^8 cm^{-2} for 1500 μm.

Comparison of EDX spectra for the initial surface of PbSe/CaF_2/Si(111) film structures and areas with PbSe nanowires showed an effect of a small change in the ratio

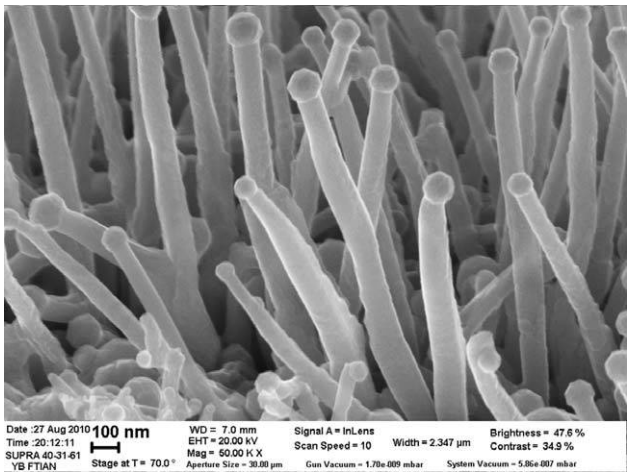

Fig. 7 Scanning electron microscopy image of the PbSe nanowires formed near the edge of a plasma-etched hole in PbSe film on CaF_2/Si(111) substrate. Sample tilt angle during imaging is 70°.

of metal–chalcogen toward increasing the Pb content at 4–5 at % for the PbSe areas under a stencil mask. At the same time, the distribution of elements on the areas under a stencil mask was uniform. Based on these data, one can assume that the fabricated 1-D nano-objects are crystalline PbSe structures, while the excessive Pb is concentrated in spherical formations.

The complex of experimental data indicates that the formation of nanowires during the plasma treatment takes place by catalytic vapor–liquid–crystal growth mechanism.[67] This process consists in the following: a droplet of a metal catalyst on the surface being in contact with the supersaturated vapor of a redeposited semiconductor material serves as a primer for an anisotropic nanowire growth.[68,69] In this case, a supersaturated lead chalcogenide vapor is created in the microgap under a stencil mask due to the high sputtering rates of PbX in Ar RF ICP. The sputtering of PbSe takes place mainly in PbSe molecules and their complexes, and the content of atomic Pb in the sputtered material is small and amounts to several at.%.[70] Since Pb has a low melting temperature, it diffuses over the heated surface under the mask and coalesces into droplets of nanometer size (which was observed during the epitaxial fabrication of PbX nanostructures and microstructures[71]). Further, when the PbX molecules redeposit on the substrate from a supersaturated vapor, there takes place a synthesis of 1-D PbSe nanostructures with Pb primers that remain at their tops.[67]

It should be noted that there also took place a redeposition of sputtered PbSe on the inner side of the mask inside the microgap forming nanostructures with 100–150 nm size with a preservation of a metal–chalcogen atomic ratio compared to the initial film, which confirms a strong effect of a sputtered material redeposition in the form of separate molecules.[67]

Fabrication of PbTe nanowires on SiO_2/Si substrates

Next, we have developed another approach to the fabrication of PbX nanowires in the microgap during sputtering based on the processes taking place on the inner side of the stencil mask. Initial PbTe single crystals with an excess of tellurium (Te) were grown by the Bridgman method.[72] Synthesized composition with p-type conductivity had excess Te-relative stoichiometry in accordance with the EDX data of 4 at.%. The grown crystals were cut perpendicular to the growth axis in order to obtain crystalline disks with the thickness of 3–5 mm, and their surface was polished with diamond paste with chemical polishing finish. The study of the crystal structure revealed that the investigated crystals were grown in the (111) growth axis and had a relatively small volume of inclusions with other orientations. The plasma processing parameters were as follows: p = 0.07 Pa, Q_{Ar} = 10 sccm, P_{sb} = 100–300 W, treatment duration = 10–60 s. During the etching process, a part of the surface of PbTe(Te) samples was closed with Si stencil masks with a natural oxide layers and with an SiO_2 layer with a thickness of 0.6 μm. Between the surface of PbTe and the mask, there was a microgap of 10–20 μm. In some experiments, the edge of the mask was protruding over the sample boundaries at a distance of about 1 mm (we describe this in more detail in Zimin et al.[73]).

Plasma processing of PbTe(Te) single crystals was characterized by intense physical sputtering and redeposition. For E_i = 200 eV, the sputtering rate was 25 ± 2 nm s^{-1}, which is 1.6 times higher than for (111)-oriented PbTe films under similar sputtering conditions. This is due to the Pb atom vacancies appearing because of the excess Te atoms in a crystal lattice. With a large deviation from the stoichiometry, the mechanical strength of the crystal is reduced, and there is a reduction in the sublimation energy of the PbTe molecules, which results in the increase of the sputtering rate with Ar^+ ions.[73]

We have found[73] that on the inner surface of the mask facing toward PbTe, there takes place a formation of various types of PbTe nanostructures due to the redeposition of the material sputtered during plasma processing. Morphologically, the obtained nanostructures could be divided into several basic types: nanocones (in the microgap area), nanocubes (also in the microgap area), and nanowires (in the areas of the protruding edge of the mask). Dimensions and density for all types of structures were dependent on processing conditions (P_{sb}, sputtering duration) and on the distance from the edge of the mask (etching step). EDX measurements have shown that for all types of nanostructure arrays, their chemical composition on a scale of ∼1 μm corresponds to PbTe. The most developed array of conical structures was obtained during treatment with P_{sb} = 100 W (Fig. 8A). Typical size of the nanocones at the base was 250 nm, height

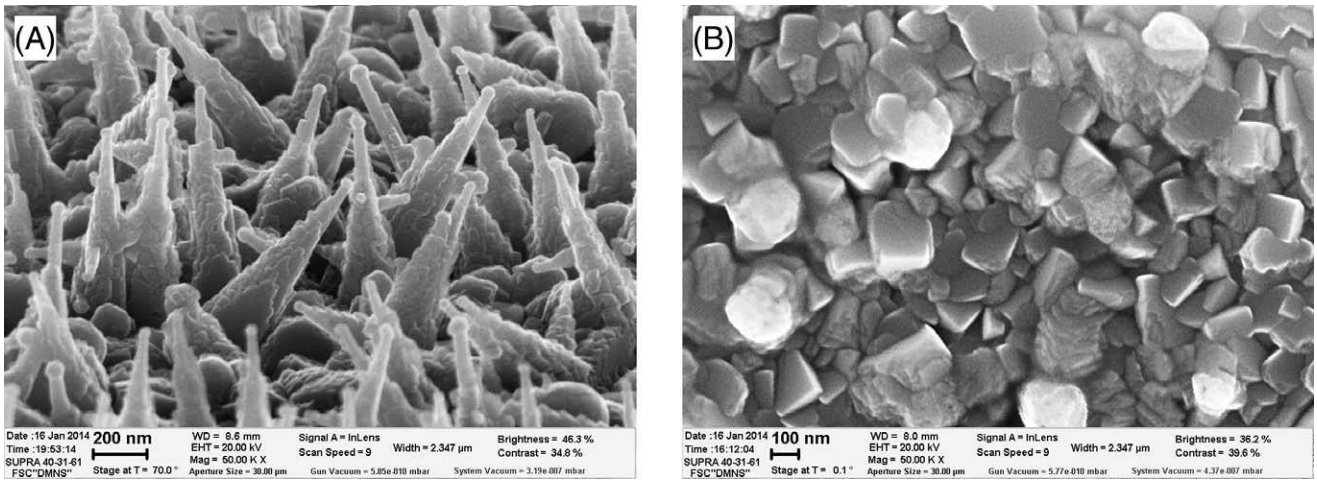

Fig. 8 PbTe nanocone (A) and nanocube (B) structures obtained on Si substrate during plasma treatment with RF bias power of 100 W and 200 W, respectively.

750 nm, and density $\sim 10^9$ cm^{-2}. The formation of nanocubes (Fig. 8B) with the edge length of 60–340 nm took place, when a high concentration of sputtered PbTe was created inside the microgap, promoting the growth of cubic structures with a minimum of free energy.

Cylindrical nanowires were effectively fabricated on the inner surface of the protruding edge of the mask for P_{sb} = 200 W. Their length gradually decreased with the distance from the outer edge of the mask. At a distance of 85 µm, the average nanowire length was 325 nm (Fig. 9), and at 170 µm, it was 75 nm. This can be explained by the shading effect, when the redeposition is stronger for the open protruding edge of the mask than for the closed microgap. The surface density of the nanowires was notably constant at 1×10^{10} cm^{-2}. The fabricated nanowires were very thin (25 nm for all the lengths), with an aspect ratio reaching 14.[73] The presence of catalyst droplets in the upper part of nanocones and nanowires indicates the formation of these structures by the vapor–liquid–solid mechanism, when the building material consists of sputtered PbTe molecules, and the droplets, in accordance with the results of previous experiments,[67] could be sublimated metallic Pb nanocrystals.

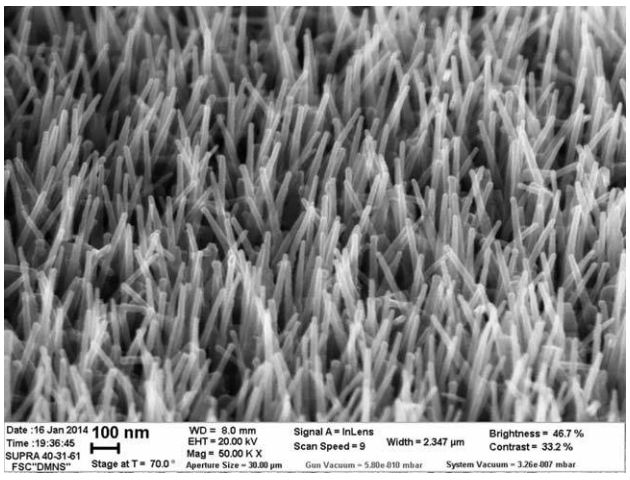

Fig. 9 PbTe nanowires formed on the overhanging part of the internal surface of the Si mask at a distance of 85 µm from the outer edge with a power RF bias of 200 W. Sample tilt angle during imaging is 70°.

CONCLUSION

A large complex of experimental research of high-density inductively coupled Ar plasma sputtering of binary IV–VI semiconductors has shown that this process has some specific features as compared to other materials. First, lead chalcogenides have a very high ICP sputtering rate values of ~ 10 nm s^{-1} (for ion energy of 150 eV and ion current density of 5.5 mA cm^{-2}[34]), surpassing many semiconductor materials. Moreover, studies showed that the sputtering rate depends on both the deviation from stoichiometry and oxygen content in the sputtered layers and may reach abnormally high values[73] or significantly decrease.[74] Second, there takes place a preferential sputtering of binary PbX molecules due to the fact that for lead chalcogenides the values of the molecule dissociation energy in the crystalline and gaseous states exceed the values of the sublimation energy. High sputtering rates and molecular sputtering make a uniquely favorable combination, which allowed forming the basis for new methods of the formation of IV–VI nanostructures on various substrates by high-density ICP sputtering, including high aspect ratio nanowires grown via vapor–liquid–solid mechanism on Si.[73] Although in this entry we focused on the processes of sputtering and nanostructuring of binary PbX materials, further experiments show great

potential for the fabrication of nanostructures by plasma sputtering for a wider range of IV–VI materials, such as PbX-based ternary solid solutions[74] and tin chalcogenide semiconductors.[75] Hopefully, the presented diverse plasma-assisted nanostructuring methods of IV–VI semiconductors would be fully realized in the fabrication of technical electronic devices for various purposes.

ACKNOWLEDGMENTS

The authors are grateful to H. Zogg (ETH, Zurich, Switzerland) for providing PbX/CaF_2/Si(111) epitaxial samples and to G.Z. Bagiyeva (Abdullaev Institute of Physics, Baku, Azerbaijan) for providing PbTe single crystal samples. This work was partially supported by Russian Foundation for Basic Research (grant 13-02-00381). Atomic force microscopy investigations were carried out with the assistance of A.O. Kucherik and S.V. Kutrovskaya (Vladimir State University, Vladimir, Russia). Scanning electron microscopy and EDX investigations using Supra 40 were carried out with the assistance of V.V. Naumov at the Facilities Sharing Centre "Diagnostics of Micro- and Nanostructures" with the financial support of the Ministry of Education and Science of the Russian Federation.

REFERENCES

1. Nimtz, G.; Schlicht, B. Narrow-gap lead salts. In *Narrow-Gap Semiconductors*; Höhler, G., Ed.; Springer Tracts in Modern Physics. Springer-Verlag: Berlin, 1983; Vol. 98, 1–117.
2. Khokhlov, D., Ed. *Lead Chalcogenides: Physics and Application*; Taylor & Francis: New York, 2003; 697 pp.
3. Abou El Ela, A.H. The absorption band edge of lead telluride films under quantum size effect. Rev. Phys. Appl. **1975**, *10*, 105–108.
4. Bartkowski, M.; Jalochowski, M.; Subotowicz, M.; Bartkowska, J. On the shape of the absorption band of very thin PbTe films in the range 1–5 eV. Thin Solid Films. **1979**, *62*, 55–60.
5. Gaponov, S.V.; Luskin, B.M.; Salashchencko, N.N. Homoepitaxial superlattices with non-oriented barrier layers. Solid State Commun. **1981**, *39*, 301–302.
6. Semonin, O.E.; Luther, J.M.; Choi, S.; Chen, H.-Y.; Gao, J.; Nozik, A.J.; Beard, M.C. Peak external photocurrent quantum efficiency exceeding 100% via MEG in a quantum dot solar cell. Science. **2011**, *334*, 1530–1533.
7. Wu, H.; Yang, Y.; Oh, E.; Lai, F.; Yu, D. Direct synthesis of high-density lead sulfide nanowires on metal thin films towards efficient infrared light conversion. Nanotechnology **2012**, *23*, 265602.
8. Wang, J.; Zens, T.; Hu, J.; Becla, P.; Kimerling, L.C.; Agarwal, A.M. Monolithically integrated, resonant-cavity-enhanced dual-band mid-infrared photodetector on silicon. Appl. Phys. Lett. **2012**, *100*, 211106.
9. Yang, S.; Zhao, N.; Zhang, L.; Zhong, H.; Liu, R.; Zou, B. Field-effect transistor-based solution-processed colloidal quantum dot photodetector with broad bandwidth into near-infrared region. Nanotechnology **2012**, *23*, 255203.
10. Dogan, S.; Bielewicz, T.; Cai, Y.; Klinke, C. Field–effect transistors made of individual colloidal PbS nanosheets. Appl. Phys. Lett. **2012**, *101*, 073102.
11. Ji, X.; Zhang, B.; Tritt, T.M.; Kolis, J.W.; Kumbhar, A. Solution-chemical syntheses of nano-structured Bi_2Te_3 and PbTe thermoelectric materials. J. Electron. Mater. **2007**, *36*, 721–726.
12. Hu, R.; Law, W.-C.; Lin, G.; Ye, L.; Liu, J.; Liu, J.; Reynolds, J.L.; Yong, K.-T. PEGylated phospholipid micelle-encapsulated near-infrared PbS quantum dots for *in vitro* and *in vivo* bioimaging. Theranostics **2012**, *2*, 723–733.
13. Wang, D.; Qian, J.; Cai, F.; He, S.; Han, S.; Mu, Y. 'Green'-synthesized near-infrared PbS quantum dots with silica–PEG dual-layer coating: Ultrastable and biocompatible optical probes for *in vivo* animal imaging. Nanotechnology **2012**, *23*, 245701.
14. Schlereth, K.-H.; Spanger, B.; Böttner, H.; Lambrecht, A.; Tacke, M. Buried waveguide double-heterostructure PbEuSe-lasers grown by MBE. Infrared Phys. **1990**, *30*, 449–454.
15. Grabecki, G.; Dietl, T.; Cieplak, M.; Plesiewicz, W.; Lenard, A.; Skoskiwicz, T.; Kamińska, E.; Piotrowska, A.; Zarecka, R.; Springholz, G.; Bauer, G. Second harmonic generation in spin-glass microstructures and fabrication of microstructures in IV-VI epilayers. Acta Phys. Pol. A **1993**, *84*, 781–784.
16. Grabecki, G.; Wróbel, J.; Dietl, T.; Papis, E.; Kamińska, E.; Piotrowska, A.; Ratuszna, A.; Springholz, G.; Bauer, G. Ballistic transport in PbTe-based nanostructures. Physica E. **2004**, *20*, 236–245.
17. Schwarzl, T.; Heiß, W.; Kocher-Oberlehner, G.; Springholz, G. CH_4/H_2 plasma etching of IV-VI semiconductor nanostructures. Semicond. Sci. Tech. **1999**, *14*, L11–L14.
18. Wu, H.F.; Zhang, H.J.; Lu, Y.H.; Si, J.X.; Li, H.Y.; Bao, S.N.; Wu, H.Z.; He, P. Ag/PbTe (111) interface behavior studied by photoemission spectroscopy. Appl. Phys. Lett. **2008**, *92*, 122112.
19. Lieberman, M.A.; Lichtenberg, A.J. *Principles of Plasma Discharges and Materials Processing*, 2nd Ed.; John Wiley & Sons, Inc.: New York, 2005.
20. Popov, O.A. *High Density Plasma Sources, Design, Physics and Performance*; Noyes: Park Ridge, NJ, 1995.
21. Ra, Y.; Chen, C.-H. Direct current bias as an ion current monitor in the transformer coupled plasma etcher. J. Vac. Sci. Technol. A **1993**, *11*, 2911–2914.
22. Cooke, M.J.; Hassall, G. Low-pressure plasma sources for etching and deposition. Plasma Sources Sci. T. **2002**, *11*, A74–A79.
23. Kawamura, E.; Vahedi, V.; Lieberman, M.A.; Birdsall, C.K. Ion energy distributions in rf sheaths: Review, analysis and simulation. Plasma Sources Sci. T. **1999**, *8*, R45–R64.
24. Sobolewski, M.A.; Olthoff, J.K.; Wang, Y. Ion energy distributions and sheath voltages in a radio-frequency-biased, inductively coupled, high-density plasma reactor. J. Appl. Phys. **1999**, *85*, 3966–3974.

25. Woodworth, J.R.; Abraham, I.C.; Riley, M.E.; Miller, P.A.; Hamilton, T.W.; Aragon, B.P.; Shul, R.J.; Willison, C.G. Ion energy distributions at rf-biased wafer surfaces. J. Vac. Sci. Technol. A **2002**, *20*, 873–887.
26. Patrick, R.; Baldwin, S.; Williams, N. Application of direct bias control in high density inductively coupled plasma etching equipment. J. Vac. Sci. Technol. A **2000**, *18*, 405–410.
27. Abdollahi-Alibeik, S.; Zheng, J.; McVittie, J.P.; Saraswat, K.C.; Gabriel, C.T.; Abraham, S.C. Modeling and simulation of feature-size-dependent etching of metal stacks. J. Vac. Sci. Technol. B **2001**, *19*, 179–185.
28. Belen, J.R.; Gomez, S.; Kiehbauch, M.; Cooperberg, D.; Aydil, E.S. Feature-scale model of Si etching in SF_6 plasma and comparison with experiments. J. Vac. Sci. Technol. A **2005**, *23*, 99–113.
29. Guo, W.; Sawin, H.H. Modeling of the angular dependence of plasma etching. J. Vac. Sci. Technol. A **2009**, *27*, 1326–1336.
30. Zimin, S.P.; Gorlachev, E.S.; Amirov, I.I.; Gerke, M.N.; Zogg, H.; Zimin, D. Role of threading dislocations during treatment of PbTe films in argon plasma. Semicond. Sci. Tech. **2007**, *22*, 929–932.
31. Zimin, S.P.; Gorlachev, E.S.; Amirov, I.I.; Gerke, M.N. Submicrometer- and nanometer-structure formation on the surface of epitaxial IV–VI semiconductor films by Ar-plasma treatment. Russian Microelectron. **2008**, *37*, 175–186.
32. Zimin, S.P.; Bogoyavlenskaya, E.A.; Gorlachev, E.S.; Naumov, V.V.; Zimin, D.; Zogg, H.; Arnold, M. Structural properties of $Pb_{1-x}Eu_xSe/CaF_2/Si(111)$. Semicond. Sci. Tech. **2007**, *22*, 1317–1322.
33. Tomas, S., III; Berg, E.W.; Pang, S.W. *In situ* fiber optic thermometry of wafer surface etched with an electron cyclotron resonance source. J. Vac. Sci. Technol. B. **1996**, *14*, 1807–1811.
34. Zimin, S.P.; Amirov, I.I.; Gorlachev, E.S. RF sputtering of epitaxial lead chalcogenide films in argon and krypton plasma. Semicond. Sci. Tech. **2011**, *26*, 055018.
35. Yu, H.W.; Youn, C.J. Etching characteristics of $Si_{1-x}Ge_x$ alloy using Cl_2 assisted Ar ion beam etching. J. Korean Phys. Soc. **1997**, *31*, 741–747.
36. Pearton, S.J.; Abernathy, C.R.; Ren, F. Dry patterning of InGaN and InAlN. Appl. Phys. Lett. **1994**, *64*, 3643–3645.
37. Ping, A.T.; Asif Khan, M.; Adesida, I. Dry etching of $Al_xGa_{1-x}N$ using chemically assisted ion beam etching. Semicond. Sci. Tech. **1997**, *12*, 133–135.
38. Vawter, G.A.; Wendt, R. Chlorine reactive ion beam etching of InSb and $InAs_{0.15}Sb_{0.85}$/InSb strained layer superlattices. Appl. Phys. Lett. **1991**, *58*, 289–291.
39. Kinoshita, H.; Ishida, T.; Kaminishi, K. Surface oxidation of GaAs and AlGaAs in low energy Ar/O_2 reactive ion beam etching. Appl. Phys. Lett. **1986**, *49*, 204–206.
40. Harper, J.M.E. *Plasma Etching: An Introduction*; Manos, D.M., Flamm, D.L., Eds.; Academic: San Diego, 1989; 391 pp.
41. Seah, M.P.; Nunney, T.S. Sputtering yields of compounds using argon ions. J. Phys. D Appl. Phys. **2010**, *43*, 253001.
42. Seah, M.P.; Clifford, C.A.; Green, F.M.; Gilmore, I.S. An accurate semi empirical equation for sputtering yields I: For argon ions. Surf. Interface Anal. **2005**, *37*, 444–458.
43. Betz, G.; Wehner, G.K. Sputtering of multicomponent materials. In *Sputtering by Particle Bombardment II*; Behrisch, R., Ed.; Springer-Verlag: Berlin, 1983; 11–90.
44. Volpyas, V.A.; Dymashevskii, P.M. A regression model for a displaced atom cascade under ion sputtering of solids. Tech. Phys. **2001**, *46*, 1347–1350.
45. Glushko, V.P., Ed. *Thermal Constants of Substances. Handbook*, Vol. 4; VINITI: Moscow, 1970; 509 pp. (in Russian).
46. Borynyak, L.A.; Velichko, A.A.; Ilyushin, V.A.; Ostertak, D.I.; Peisakhovich, Y.G.; Filimonova, N.I. Electron-beam-induced modification of PbSnTe surface morphology under HEED monitoring of MBE growth. Russian Microelectron. **2008**, *37*, 146–156.
47. Springholz, G.; Bauer, G. Molecular beam epitaxy of IV–VI semiconductor hetero- and nano structures. Phys. Status Solidi B. **2007**, *244*, 2752–2767.
48. National Physical Laboratory Sputter Yield Values. Available at http://www.npl.co.uk/science-technology/surface-and-nanoanalysis/services/sputter-yield-values (accessed July 2015).
49. Sigmund, P. Theory of sputtering. I. Sputtering yield of amorphous and polycrystalline targets. Phys. Rev. **1969**, *184*, 383–416.
50. Zimin, S.P.; Gorlachev, E.S.; Amirov, I.I.; Zogg, H.; Abramof, E.; Rappl, P.H.O. Sputtering rates of lead chalcogenide-based ternary solid solutions during inductively coupled argon plasma treatment. Semicond. Sci. Tech. **2011**, *26*, 105003.
51. Amirov, I.I.; Zimin, S.P.; Gorlachev, E.S.; Naumov, V.V.; Abramof, E.; Rappl, P.H.O. Investigations of the inductively coupled argon plasma sputtering of $Pb_{1-x}Sn_xTe$ ternary solid solution. J. Surf. Invest. **2012**, *6*, 643–646.
52. Zogg, H.; Maissen, C.; Blunier, S.; Teodoropol, S.; Overney, R.M.; Richmond, T.; Tomm, J.W. Thermal mismatch strain relaxation mechanisms in heteroepitaxial lead-chalcogenide layers on Si-substrates. Semicond. Sci. Tech. **1993**, *8*, S337–S341.
53. Zimin, S.P.; Gorlachev, E.S.; Amirov, I.I.; Zogg, H. Micromasking effect and nanostructures self-formation on the surface of lead chalcogenide epitaxial films on Si substrates during argon plasma treatment. J. Phys. D Appl. Phys. **2009**, *42*, 165205.
54. Oehrlein, G.S.; Rembetski, J.F.; Payne, E.H. Study of sidewall passivation and microscopic silicon roughness phenomena in chlorine-based reactive ion etching of silicon trenches. J. Vac. Sci. Technol. B. **1990**, *8*, 1199–1211.
55. Craighead, H.G.; Howard, R.E.; Tennant, D.M. Textured thin film Si solar selective absorbers using reactive ion etching. Appl. Phys. Lett. **1980**, *37*, 653–656.
56. She, J.C.; Deng, S.Z.; Xu, N.S.; Yao, R.H.; Chen, J. Fabrication of vertically aligned Si nanowires and their application in a gated field emission device. Appl. Phys. Lett. **2006**, *88*, 013112.
57. Steckl, A.J.; Yih, P.H. Residue free reactive ion etching of beta SiC in CHF_3/O_2 with H_2 additive. Appl. Phys. Lett. **1992**, *60*, 1966–1968.
58. Choi, D.Y.; Lee, J.H.; Kim, D.S.; Jung, S.T. Formation of plasma induced surface damage in silica glass etching for optical waveguides. J. Appl. Phys. **2004**, *95*, 8400–8407.
59. Ramos, R.; Cunge, G.; Pelissier, B.; Joubert, O. Cleaning aluminum fluoride coatings from plasma reactor walls in

$SiCl_4/Cl_2$ plasmas. Plasma. Sources Sci. T. **2007**, *16*, 711–715.
60. Tsui, B.-Y.; Yang, T.-J.; Ku, T.-K. Impact of interface nature on deep sub-micron Al plug resistance. Microelectron. Reliab. **2001**, *41*, 1889–1896.
61. Wu, H.F.; Zhang, H.J.; Lu, Y.H.; Xu, T.N.; Si, J.X.; Li, H.Y.; Bao, S.N.; Wu, H.Z.; He, P. Scanning tunneling microscopy of epitaxial growth of PbSe thin film on BaF_2(111). J. Cryst. Growth **2006**, *294*, 179–183.
62. Xu, T.N.; Wu, H.Z.; Si, J.X.; Cao, C.F. Observation of triangle pits in PbSe grown by molecular beam epitaxy. Appl. Surf. Sci. **2007**, *253*, 5457–5461.
63. Wise, F.W. Lead salt quantum dots: The limit of strong quantum confinement. Acc. Chem. Res. **2000**, *33*, 773–780.
64. Alchalabi, K.; Zimin, D.; Kostorz, G.; Zogg, H. Self assembled semiconductor quantum dots with nearly uniform sizes. Phys. Rev. Lett. **2003**, *90*, 026104.
65. Ostrikov, K.; Murphy, A.B. Plasma aided nanofabrication: Where is the cutting edge? J. Phys. D Appl. Phys. **2007**, *40*, 2223–2241.
66. Levchenko, I.; Ostrikov, K. Nanostructures of various dimensionalities from plasma and neutral fluxes. J. Phys. D Appl. Phys. **2007**, *40*, 2308–2319.
67. Zimin, S.P.; Gorlachev, E.S.; Amirov, I.I.; Naumov, V.V. Lead selenide nanowire growth by vapor-liquid-solid mechanism under mask during plasma processing. Tech. Phys. Lett. **2011**, *37*, 929–931.
68. Wagner, R.S.; Ellis, W.C. Vapor liquid solid mechanism of single crystal growth. Appl. Phys. Lett. **1964**, *4*, 89–90.
69. Misra, S.; Yu, L.; Chen, W.; Foldyna, M.; Roca i Cabarrocas, P. A review on plasma-assisted VLS synthesis of silicon nanowires and radial junction solar cells. J. Phys. D Appl. Phys. **2014**, *47*, 393001.
70. Plyatsko, S.V. Laser-modulated epitaxy of lead telluride. Semiconductors **1998**, *32*, 270–273.
71. Ma, J.G.; Curtis, M.E.; Zurbuchen, M.A.; Keay, J.C.; Weng, B.B.; Li, D.H.; Zhao, F.H.; Johnson, M.B.; Shi, Z. Growth mechanism of cuboid growth pits in lead selenide epilayers grown by molecular beam epitaxy. J. Phys. D Appl. Phys. **2010**, *43*, 455411.
72. Bagiyeva, G.Z.; Mustafayev, N.B.; Abdinova, G.D.; Abdinov, D.S. Electrical properties of PbTe single crystals with excess tellurium. Semiconductors **2011**, *45*, 1391–1394.
73. Zimin, S.P.; Gorlachev, E.S.; Amirov, I.I.; Naumov, V.V.; Bagiyeva, G.Z. Application of abnormally high sputtering rate of PbTe(Te) single crystals during inductively coupled argon plasma treatment for fabrication of nanostructures. Semicond. Sci. Tech. **2015**, *30*, 035017.
74. Zimin, S.P.; Gorlachev, E.S.; Gremenok, V.F.; Tsyrelchuk, I.N.; Naumov, V.V.; Amirov, I.I.; Dubov, G.A. Plasma sputtering of polycrystalline $Pb_{1-x}Sn_xTe$ thin films grown on glass substrates using hot wall deposition. Semicond. Sci. Tech. **2014**, *29*, 075020.
75. Zimin, S.P.; Gorlachev, E.S.; Amirov, I.I.; Naumov, V.V.; Dubov, G.A.; Gremenok, V.F.; Bashkirov, S.A. Investigations of nanocrystalline SnS films' surface morphology modification during inductively coupled argon plasma sputtering. Semicond. Sci. Tech. **2014**, *29*, 015009.